



www.JCRonline.org

REVIEW ARTICLES



www.cerf-jcr.org

Potential Applications of HypsIRI for the Observation of Sea-Margin Processes

Young-Heon Jo^{†*}, Hyun-Cheol Kim[‡], Chuanmin Hu[§], Victor V. Klemas^{††}, and Kevin R. Turpie^{‡‡}

[†]Department of Oceanography
Pusan National University
Busan 46241, South Korea

[‡]Korea Polar Research Institute
Incheon 21990, South Korea

[§]College of Marine Science
University of South Florida
St. Petersburg, FL 33701, U.S.A.

^{††}College of Earth Ocean and Environment
University of Delaware
Newark, DE 19716, U.S.A.

^{‡‡}Joint Center for Earth Systems
and Technology
University of Maryland
Baltimore County, MD 21228, U.S.A.

ABSTRACT

Jo, Y.-H.; Kim, H.-C.; Hu, C.; Klemas, V.V., and Turpie, K.R., 2019. Potential applications of HypsIRI for the observation of sea-margin processes. *Journal of Coastal Research*, 35(1), 227–239. Coconut Creek (Florida), ISSN 0749-0208.

The Hyperspectral Infrared Imager (HypsIRI) mission will observe the effects of future environmental changes upon the world's ecosystems. Among other applications, this paper reviews three different sea-margin processes that can be monitored by the HypsIRI spectrometer, *i.e.* groundwater and surface-water discharge, meltwater-pond formation, and shoreline delineation. Groundwater and surface-water discharge to coastal regions affects local ecological conditions through changes in the local temperature, salinity, and nutrient load. Water-quality changes and temperature variability resulting from such discharge can be estimated from observation in the visible-to-shortwave-infrared (VSWIR) and the mid- and thermal-infrared (TIR) regions, respectively. The processes of meltwater forming ponds and entering the sea have unique ecological characteristics and are of additional interest because they are also highly subject to climate change. HypsIRI can use TIR to observe the spatial distribution of meltwater, whereas its VSWIR spectrometer can be used to quantify the changes of phytoplankton pigments (*e.g.*, chlorophyll *a*). Quantifying sea-margin changes requires accurate delineation of margin positions wherein tidal influence is minimal. Since the HypsIRI VSWIR data cover a wide spectral range and offer high spatial resolution, they are particularly suitable for shoreline delineation/change detection, as well as flood mapping. The signal-to-noise ratio of HypsIRI is expected to be comparable to that of the Hyperspectral Imager for the Coastal Ocean and much higher than that of Hyperion and Landsat Enhanced Thermal Mapper Plus, making it suitable for studying optically complex coastal aquatic environments. Herein, using examples from existing satellite sensors, HypsIRI's potential to study these complex sea-margin processes is presented and discussed.

ADDITIONAL INDEX WORDS: *Hyperspectral Infrared Imager, groundwater, ice, shoreline remote sensing.*

INTRODUCTION

The margins of a sea are not static, and they are subject to natural and human changes. Accordingly, observations of the boundaries between water and land (Leote, Ibanhez Severino, and Rocha, 2008) and water and ice (Muller-Karger, 1984; Muller-Karger and Alexander, 1987; Muller-Karger, McClain, and Ray, 1987; Muller-Karger *et al.*, 1990) can reveal changes in the margin position and environmental characteristics such as cross-margin material flux (dissolved or suspended), littoral currents, and near-margin ecological attributes. These sea-margin processes can occur on gradual (*e.g.*, resulting from sea-level rise) or dramatic (*e.g.*, disturbances such as severe storms)

timescales. Thus, in the following paragraphs, three different sea-margin processes are reviewed that can be observed with the various remote-sensing sensors: groundwater and surface-water discharge, meltwater-pond formation, and shoreline delineation.

First, the variation of terrestrial freshwater flux across the boundary via groundwater or surface-water discharge can influence the transport of nutrient flux into coastal waters (Childers *et al.*, 2006). In particular, the increased supply of nutrients following groundwater discharge after hurricanes has been speculated to be linked to harmful algal blooms in coastal waters off central Florida (Hu, Muller-Karger, and Swarzenski, 2006) and Masan Bay in South Korea (Lee and Kim, 2007), and it has been interpreted as a potential precursor to increased bacterial concentrations in the surf zone (Boehm, Shellanbarger, and Paytan, 2004). However, detecting locations and quantifying the contributions of groundwater

DOI: 10.2112/JCOASTRES-D-17-00089.1 received 21 May 2017; accepted in revision 24 February 2018; corrected proofs received 26 March 2018; published pre-print online 16 April 2018.

*Corresponding author: joyoung@pusan.ac.kr

©Coastal Education and Research Foundation, Inc. 2019

discharge into coastal waters are challenging because field observations are limited. Thus, remote sensing has proven to be useful for monitoring groundwater discharge using temperature differences between coastal water and groundwater (Schubert *et al.*, 2014).

Groundwater discharge has also been considered as a potentially significant source of diffuse nutrients, dissolved substances, and diffuse pollution in coastal regions (Leote, Ibanhez Severino, and Rocha, 2008). Anthropogenic materials, such as pesticides, herbicides, chemical fertilizers, and petroleum products, are common groundwater pollutants (Nowack, Xue, and Sigg, 1997). These pollutants usually enter groundwater when polluted water percolates down from the ground surface (Hildebrandt *et al.*, 2008). Relatively small groundwater discharge rates can deliver comparatively large quantities of nutrients and pollutants to coastal areas (Konstantinou, Hela, and Albanis, 2006; Sangodoyin and Agbawhe, 1992). Leaking underground storage tanks are another major source of groundwater pollution (Grose *et al.*, 1995; Moseley and Meyer, 1992). It is estimated that there are millions of underground storage tanks in the United States. Agricultural and lawn applications of fertilizers also present a major diffuse source of nutrients that can enter coastal and inland waters through groundwater discharge. Accordingly, monitoring and detecting contaminated groundwater discharge into coastal regions are critically important for sustaining a healthy ecosystem.

Groundwater discharge can be observed as follows. The temperature of such groundwater is almost constant throughout the year, and the use of thermal remote sensing to delineate groundwater discharge to coastal regions has been reported. Research has been conducted in Chesapeake Bay (Banks, Paylor, and Hughes, 1996), Cape Cod (Portnoy *et al.*, 1998), Delaware's Inland Bays (McKenna, Andres, and DeLiberty, 2001; Ullman and Miller, 2004; Wang, McKenna, and DeLiberty, 2008), the Great Bay Estuary (New Hampshire) and Waquiot Bay (Massachusetts) (Roseen, Brannaka, and Balles-tero, 2001), and Hawaii (Johnson *et al.*, 2008).

Second, another relevant sea-margin process is ice-margin environmental change. Global warming is altering the timing, rate, and extent of formation, melting, and breaking of ice packs and ice shelves at high latitudes. As ice melts, freshwater strongly affects the phytoplankton ecology. Phytoplankton form blooms within the ice near its edges (Muller-Karger, 1984; Muller-Karger and Alexander, 1987; Muller-Karger, McClain, and Ray, 1987; Muller-Karger *et al.*, 1990), and these blooms can be strongly affected by climate change (Perrette *et al.*, 2011). Accordingly, it is critically important to study phytoplankton in ice pools (Lee *et al.*, 2012) using meltwater optical properties, which can provide information regarding the resulting biological response through observation of phytoplankton-pigment changes and changes in that environment as a result of climate change.

Ice-margin processes can be observed as follows. Several different remote-sensing observations have been performed on the ice margin. While Drüe and Heinemann (2005) used the Moderate Resolution Imaging Spectroradiometer (MODIS) and *in situ* examination to assess sea-ice concentrations, Shi *et al.* (2012) extracted sea-ice information from the surface temper-

ature based on the National Oceanic and Atmospheric Administration (NOAA) Advanced Very High Resolution Radiometer (AVHRR) and obtained the relationship between ice thickness and reflectivity by an empirical formula. Furthermore, while Meyer *et al.* (2011) introduced an approach to map the fast-ice extent on land using L-band synthetic aperture radar (SAR), Ozsoy-Cicek *et al.* (2011) verified by field survey that active microwaves can monitor the ice edge and floating ice.

Shoreline variation is the third sea-margin process that can cause changes to littoral and coastal ecologies, beach nourishment, and coastal currents and can affect navigation and coastal properties. Numerous natural and anthropogenic processes can result in shoreline changes, including sea-level change, hurricanes, coastal circulation, riverine-discharge patterns, beach nourishment, and sand dredging (Wu, 2007). Such changes may affect coastal-zone resilience against storm surges and flooding, with significant impacts upon ecosystem health and species diversity (Desantis *et al.*, 2007). Such changes may also have important socioeconomic consequences on local residents and tourism. Thus, it is important to assess shoreline changes periodically for management decisions such as beach nourishment (*e.g.*, location and frequency). Likewise, flooding (or drought) events from either extreme weather or poor management (*e.g.*, damage of a levee) often lead to property loss, economic hardship, and risk to human lives. In addition, rapid changes of dry/wet conditions can change the surface-exposure periods to water and sunlight, therefore also influencing the local ecosystem (*e.g.*, Kanai *et al.*, 2002). Accurate estimation of flood patterns is an important first step in flood-control, search-and-rescue, land-use-planning, and ecological-conservation efforts.

It is widely accepted that sea level is rising worldwide, with a current average rise of 3.1 mm/y (Church *et al.*, 2010; Song and Colberg, 2011; Stammer *et al.*, 2013). The effects of sea-level rise include an increase in the impact of storm surges and wave action, increased inundation events in flood-prone areas, loss of tidal wetlands and riparian habitats, and increased vulnerability of upland areas (Klemas, 2009). Sea-level rise can cause higher water tables and saltwater intrusion, adversely affecting habitats, drinking water, irrigation systems, and septic systems (Chang *et al.*, 2011).

The shoreline changes can be observed as follows. Shoreline changes can be obtained from ground surveys (Morton *et al.*, 1993), airborne polarimetric SAR (Jeremy *et al.*, 2001), and contouring methods with LIDAR digital elevation models (DEMs) (Li, Ma, and Di, 2002; Liu, Sherman, and Gu, 2007; Robertson *et al.*, 2004; Stockdon *et al.*, 2002; White, 2007; White *et al.*, 2010), as well as a combination of LIDAR DEMs, satellite images, and orthoimages (Lee, Cheng, and Li, 2010; Lee, Wu, and Li, 2009). At present, the most common means of extracting shorelines is based on spaceborne sensors. Such methods include intertidal DEMs interpolated from water-level-referenced instantaneous-shoreline information (Hoja *et al.*, 2000), intertidal DEMs using the waterline method based on European Remote Sensing-1 (ESR-1) SAR images (Mason, Davenport, and Flather, 1997; Mason *et al.*, 1995, 1998, 2001), DEMs generated from IKONOS imagery (Muslim and Foody, 2008), and snake-based tide-coordinated shorelines (Li *et al.*,

2006). Furthermore, different spatial and temporal resolutions of satellite imagery have also been used for shoreline-change detection (Zimmerman and Bijker, 2004). Accordingly, the shorelines estimated from remote-sensing satellite-sensor imagery have been frequently updated (Cendrero and Fischer, 1997; Dekker *et al.*, 1992; LaValle and Lakhan, 2000; Stauble, 2003).

It is worth noting that while multispectral remote-sensing observations could provide optical properties of sea-surface changes, microwave and RADAR/LiDAR measurements enable estimations to be made for sea-ice concentrations along sea-ice boundaries and sea-surface roughness resulting from groundwater discharge near shores, which enable three sea-margin processes to be studied, respectively. Furthermore, the hyperspectral measurements can provide better spatial and spectral resolutions to determine the characteristics of sea-surface information, meltwater-pond formation, and shoreline changes (including mudflat constituents). Therefore, integrating all remote-sensing measurements (multispectral, microwave, RADAR/LiDAR, and hyperspectral measurements) will allow understanding of very detailed small-spatial-scale sea-margin processes, but also large features of sea-margin boundaries.

Hyperspectral remote sensing is an efficient tool for observing the changes that occur on these boundaries at both local and synoptic scales. The National Aeronautics and Space Administration (NASA) of the United States launched the first spaceborne hyperspectral sensor, Hyperion, with 220 contiguous spectral bands, in 2000 (<https://eo1.usgs.gov/sensors/hyperion>); in 2001, the European Space Agency launched the Compact High Resolution Imaging Spectrometer (CHRIS), a programmable sensor with up to 63 bands (<https://earth.esa.int/web/guest/missions/esa-operational-eo-missions/proba/instruments/chris>), and the Naval Research Laboratory built and launched the Hyperspectral Imager for the Coastal Ocean (HICO) in 2009 (<http://hico.coas.oregonstate.edu/>). Except for HICO, none of the spaceborne hyperspectral sensors launched so far has been designed to have a signal-to-noise ratio (SNR) optimized for the optically complex coastal aquatic environment. HICO is a low-cost prototype sensor that was developed as a demonstration mission with on-demand image acquisition and was not designed to provide global coverage on a regular basis. Unfortunately, HICO ended operations due to an X-class solar storm in September 2014 (<http://hico.coas.oregonstate.edu/>) (Table 1).

Although observations of specific targets depend on different spatial, temporal, and spectral resolutions, the Hyperspectral Infrared Imager (HyspIRI), a planned mission, can provide global coverage at a high spectral resolution (HyspIRI-TIR Science Working Group Report, 2007). The HyspIRI mission includes two instruments: an imaging spectrometer for observations in the visible-to-short-wave-infrared (VSWIR) region (380–2500 nm) in 10 nm contiguous bands, and a multispectral imager for observations in the mid- and thermal-infrared (TIR: 3–12 μm) bands. The VSWIR and TIR instruments both have a minimum spatial resolution of 30 m. The VSWIR will have a revisit period of 16 days, and the TIR will have a revisit period of 5 days (Table 1). The comparisons between different sensors and HyspIRI are summarized in Table 2.

In addition, with HyspIRI's high spectral resolution combined with a relatively high SNR, the sensor can provide information regarding optically active constituents of water columns, thus allowing for measurement of the concentrations of phytoplankton pigments, colored dissolved organic matter, and suspended-particle concentrations and compositions (Devred *et al.*, 2013). Combined with simultaneous measurements of surface temperature from HyspIRI's thermal bands, episodic observations of the biological response to terrestrial groundwater and surface-water nutrient flux or meltwater can be made. Furthermore, under ideal conditions, shorelines can also be discriminated by near-infrared (NIR) or short-wave-infrared (SWIR) observation, since deep water has very low NIR reflectance, and, conversely, most beaches along shorelines tend to be relatively bright (*e.g.*, whether they are composed of sand or have a heavy vegetation cover).

Although various topics for HyspIRI applications were reviewed extensively in a special issue of *Remote Sensing of Environment* (Hochberg *et al.*, 2015), this paper mainly focuses on three different sea-margin processes, evaluating how HyspIRI addresses these problems with existing satellite sensors using specific algorithms. In particular, the advantages of using HyspIRI's hyperspectral bands to extract three different sea-margin processes are discussed in the following section. These processes include (1) groundwater and surface-water discharge, with examples of Landsat thermal measurements and yellow fluorescence from HICO in the coastal regions, (2) ice-margin environment change, with examples of the Greenland Ice Sheet and sea ice from MODIS and sea-ice concentration from the Special Sensor Microwave Imager (SSM/I), and (3) shoreline changes, with examples of shoreline change measurements from Landsat, and mudflat characteristics, shallow-water bathymetry, and seagrass leaf area index (LAI) from the Hyperspectral Imager. Since HyspIRI may be of use in geomorphology research, a discussion of its challenges, limitations, and potential solutions is also presented, followed by an overall conclusion.

RESULTS

In this section, prospective HyspIRI observations of sea-margin processes are reviewed. These processes include groundwater and surface-water discharge, changes to the ice-margin environment, and shoreline changes and floods.

Groundwater and Surface-Water Discharge

Figure 1 shows groundwater discharge locations that have been identified with Landsat thermal data over Delaware on the northern shore of Rehoboth Bay west of the Lewes, in the Rehoboth Canal, on the Herring and Guinea Creeks, and on the north shore of Indian River Bay near Oak Orchard (Wang, McKenna, and DeLiberty, 2008). The identified locations are consistent with other measurements of groundwater discharge. However, to analyze the ecological impact of groundwater and surface-water discharge upon complex coastal water areas, biogeochemical water constituents need to be observed. Since the discharged groundwater can be easily mixed with coastal water, temperature variability measured by Landsat alone is insufficient, suggesting that more spectral measurements are required to estimate various biogeochemical water properties

Table 1. Specifications of five satellite sensors.

Specification	Landsat [†]	Hyperion [‡] (SWIR and VNIR)	HICO [§]	MODIS Aqua	HyspIRI [¶]	
					VSWIR	TIR
History	1972–	21 November 2000	2009–2014	2002–	Planned 2020	
Spatial resolution	30 m for Landsat 8 100 m for TIRS of Landsat 8	30 m	90 m	250 m (bands 1–2) 500 m (bands 3–7) 1 km (bands 8–36)	30 m (depth <50 m) 1 km (depth >50 m)	60 m (depth <50 m) 1 km (depth >50 m)
Temporal resolution	16 days	16 days 7.5 × 200 km scene per orbit	50 × 200 km scene per orbit	1–2 days	16 days Rapid response 3 days	5 days Rapid response 3 days
Spectral bands	11 (Landsat 8)	220	128	36	213	7
Spectral wavelength range	483–2215 nm	0.4–2.5 μm	380–960 nm	Multispectrum	380–2500 nm	3–12 μm
Bandwidth		10 nm	5.7 nm	Varies	10 nm	0.08–0.52 μm
Signal-to-noise ratio		161 (550 nm) 147 (700 nm) 110 (1125 nm) 40 (2125 nm)	>200 to 1	880 (405–420 nm) 516 (862–877 nm)	SNR of HyspIRI is better than that of Hyperion and comparable to that of HICO	

[†]<http://landsat.gsfc.nasa.gov/>

[‡]<http://www.crisp.nus.edu.sg/~research/tutorial/eo1.htm>

[§]<http://hico.coas.oregonstate.edu/>

^{||}<http://modis.gsfc.nasa.gov/about/specifications.php>

[¶]Devred et al. (2013)

(Becker, 2006). In other words, to determine the spatial extent of groundwater discharge in such a region, many remote-sensing observations (or field surveys for surface-water temperature) are required. In particular, Devred et al. (2013) proposed applications of HyspIRI to coastal and inland water observation. The present study provides an overview of how the HyspIRI mission could enable the retrieval of new aquatic-biophysical products.

The difficulty in quantifying the diffuse sources of pollutants into estuarine and lacustrine waters has limited the regulation and management of coastal and inland water quality (Barbier, 2008). The combination of high-spatial-resolution hyperspectral VSWIR and thermal information from HyspIRI offers a unique opportunity to map groundwater and surface-water discharge sites and their effects upon surrounding biological processes. Furthermore, the combination of HyspIRI data, GIS data, and field measurements can offer an unprecedented capability to characterize groundwater-flow systems and discharge-recharge relationships.

Another example is the detection of a *Karina brevis* (red tide) bloom due to groundwater discharge in regions at less than 50

m depth on the west Florida shelf using MODIS imagery (Hu, Muller-Karger, and Swarzenski, 2006). Hu, Muller-Karger, and Swarzenski noted that several factors may have contributed to the 2005 red tide, including the 2004 hurricanes and their associated heavy rain, runoff, and submarine (below the ocean floor) groundwater discharge. They used MODIS imagery and observations from ships, buoys from NOAA, and geochemical tracers to study the red tide. Although it would be difficult to assess groundwater discharge directly using HyspIRI measurements for this region, the mission's high spatial and spectral resolutions enable observations of both *K. brevis* and *Trichodesmium* (a precursor to *K. brevis*) blooms at higher resolution compared to MODIS, thereby providing unprecedented information on studies of nutrient and carbon cycles in coastal oceans, with submarine-groundwater discharge being an integrated component of these cycles.

A specific example is shown in Figure 2. Figure 2a shows a type of bloom that cannot be distinguished by MODIS's limited spectral bands; Figure 2b presents a hyperspectral HICO image showing characteristic yellow fluorescence due to the phycoerythrin pigment within the dominant chloro-

Table 2. Comparisons between HyspIRI and other sensors.

Three Marginal Sea Processes	Necessary Observations	Potential Satellite Sensors			
		Landsat	Hyperion	HICO	MODIS
Groundwater discharge	SST and biogeochemical constituents	Landsat is comparable to HyspIRI, but no biogeochemical	HyspIRI VSWIR provides complete coverage over the entire globe every 16 days. It would take Hyperion 100 years to acquire what HyspIRI measures in 1 year. HyspIRI TIR provides complete coverage every 5 days. [†]	HICO is comparable to HyspIRI, but no thermal information available.	MODIS is not comparable to HyspIRI for spatial and spectral resolution.
Ice margin	SST and Chl <i>a</i>	constituent			
Shoreline changes	Water-land boundary and sediment characteristics	measurements available.			

SNR of HyspIRI is better than that of Hyperion and MODIS (Hu et al., 2012, their figure 8) and Landsat ETM+ (Hu et al., 2012, their figure 7) and comparable to that of HICO (Lucke et al., 2011).

[†]http://hyspiri.jpl.nasa.gov/downloads/2014_Workshop/day1/3_Pres_HyspIRI_WS14_Comprehensive_Report_overview_20141013b.pdf

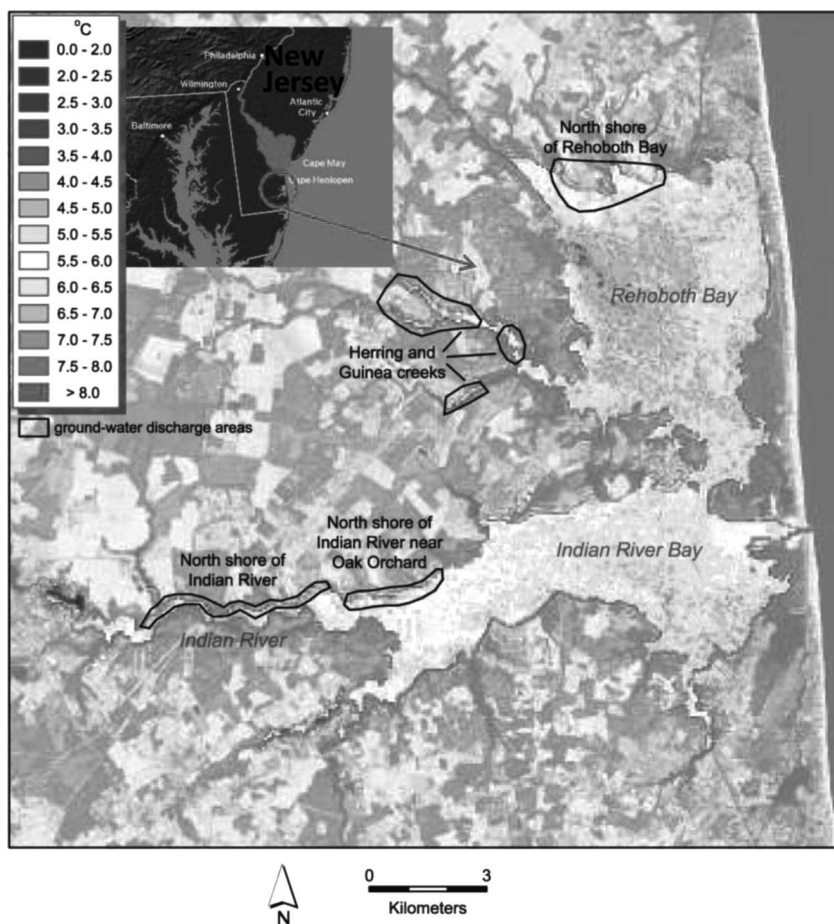


Figure 1. Groundwater-discharge areas in the Delaware Inland Bays identified using Landsat-7 imagery acquired on 19 February 2002. This figure is adopted from Wang, McKenna, and DeLiberty (2008).

plasts of the ciliate *Mesodinium rubrum*. The higher spatial resolution of the HICO image allows small, concentrated patches of yellow-fluorescing *Mesodinium* to be observed. Due to limitations in spectral resolution, prior remote-sensing (such as MODIS) studies of *M. rubrum* have been based on either nonspecific markers of darkened water or on general absorption of green light (520–600 nm) (Garcia, Purdie, and Robinson, 1993).

In certain cases, hyperspectral measurements can help to reveal comprehensive changes in the coastal regions due to groundwater discharge. For instance, the impacts of groundwater upon coastal ecosystems were also studied using the Compact Airborne Spectrographic Imager 550 (CASI-550) sensors (Kolokoussis *et al.*, 2011). That study used turbidity-related inherent optical properties (IOPs) for water to demonstrate that turbidity can be effectively estimated using certain band ratios or feature-extraction methods and concluded that the hyperspectral data were the most appropriate for detecting relatively small submarine-groundwater discharges, which were not detected under thermal imagery, due to the increase in turbidity that these discharges cause. This was

confirmed by the strong correlations between the hyperspectral data and the *in situ*-measured turbidity-related water IOPs.

Likewise, since groundwater discharge affects water quality in coastal regions, hyperspectral remote sensing has been used to monitor water quality-related properties (Ammenberg *et al.*, 2002; Flink, Lindell, and Ostlund, 2001; Galvao *et al.*, 2003; Gould and Arnone, 1997; Hakvoort *et al.*, 2002; Kallio *et al.*, 2001; Lee *et al.*, 1994; Ostlund *et al.*, 2001; Yang and Pan, 2007). These properties can be used to study the possible consequences of groundwater discharge, provided that such discharge data can be obtained from other measurements or models.

As a result, HyspIRI measurements with two instruments, VSWIR and TIR, will enable groundwater- and surface-water discharge areas to be identified and the ecological changes in the complex coastal water to be analyzed.

Ice-Margin Environment

Melting ice around the polar regions is not a local but a global phenomenon, thus requiring synoptic remote-sensing assessment. Figure 3 shows MODIS/Terra imagery of the Greenland Ice Sheet, taken on 30 August 2008. The image reveals the

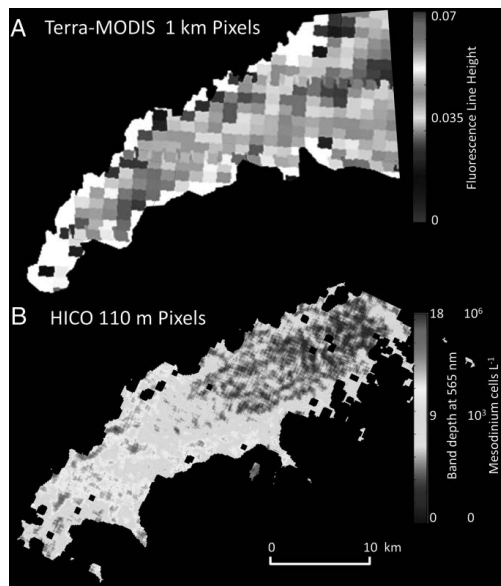


Figure 2. (a) Estimation of fluorescence line height for Chl *a* fluorescence patches at a resolution of 1 km from the MODIS Terra sensor at west Long Island Sound on 23 September 2012. (b) *Mesodinium* cells in HICO imagery from the International Space Station reveal characteristic yellow fluorescence on 23 September 2012. This figure was adapted from H. Dierssen.

eastern margin of the ice sheet, bare rocks of the coastline, and fragments of sea ice floating on the ocean surface. The ice sheet's margin appears pale blue-gray, suggesting that it may be saturated with water. Deeper blue pools of standing meltwater dot the ice sheet's surface. To monitor the melt pond, the 250 m spatial resolution of MODIS's true-color image may be insufficient. Thus, higher spatial and spectral resolu-

tions provided by HypsIRI can enhance the ability to monitor melt ponds as well as ice margins.

The top panel of Figure 4 shows swirls of sea ice along the crumbling edge of the consolidated ice pack, while the bottom panel reveals a bloom in the Chukchi Sea northwest of Alaska on 10 July 2011. The image is based on satellite ocean-color observations of the reflected light, which were used with inversion algorithms to estimate the chlorophyll concentration (CHL). Algal biomass was exported from melting ice or ponds (Boetius *et al.*, 2013; Lee *et al.*, 2012).

To facilitate monitoring of this important phenomenon, HypsIRI provides hyperspectral and high-resolution data (30 m), thus removing uncertainties in atmospheric correction and bio-optical inversion and leading to a more accurate assessment of blooms near the ice edge. David *et al.* (2015) introduced the atmospheric correction based on the theoretical approach, which is grounded in the atmospheric-removal (ATREM) algorithm. Combined with other data such as sea-surface temperature (SST), which can be estimated by HypsIRI or other satellites, HypsIRI provides a powerful tool for quantifying the impact of ice melt upon the nearby water.

Monitoring the ice-margin environment, including melted areas, is very important for predicting future climate change. To detect melted areas, Chylek *et al.* (2007) reported the melt-area-detection index (MADI) using MODIS measurements, where:

$$\text{MADI} = R_{670}/R_{2100} \quad (1)$$

Here, R_{670} is the reflectance in MODIS band 1 (645 nm), and R_{2100} is the reflectance in band 7 (2300 nm). Similarly, MADI based on HypsIRI measurements can be employed to obtain better results because of HypsIRI's higher resolution.

In addition to MADI from Eq. (1) for detecting melting areas, hyperspectral remote sensing is very promising for studying not only the structure of the ice margin but also the biogeochemical constituents resulting from melting ice. Hyper-

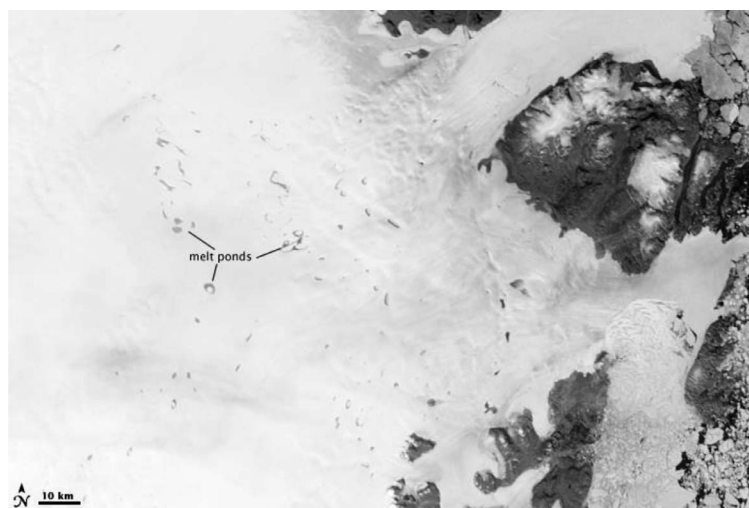


Figure 3. MODIS imagery acquired on 30 August 2008 over northeastern Greenland. Several melt ponds are indicated. Deeper blue pools of standing meltwater dot the ice sheet's surface. (<http://earthobservatory.nasa.gov/IOTD/view.php?id=35696>)

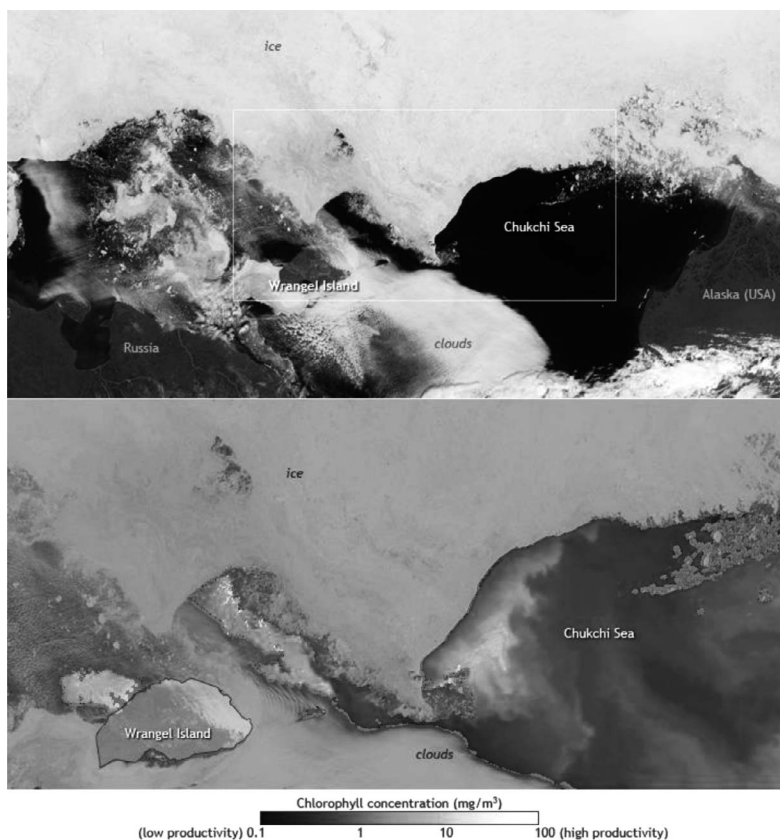


Figure 4. MODIS images showing a bloom in the Chukchi Sea northwest of Alaska on 10 July 2011. The top panel shows a red-green-blue (RGB) composite image, and the lower panel shows chlorophyll concentrations. Image is courtesy of Jesse Allen, NASA Earth Observatory team (<http://www.climate.gov/news-features/features/melt-pond-skylights-enable-massive-under-ice-bloom-arctic>).

spectral remote images contain nearly continuous spectral information and abundant spatial information; thus, hyperspectral remote sensing offers higher target-recognition capa-

bilities and can significantly improve target-detection accuracy. Many methods have been developed to classify hyperspectral images, which can be grouped into two main

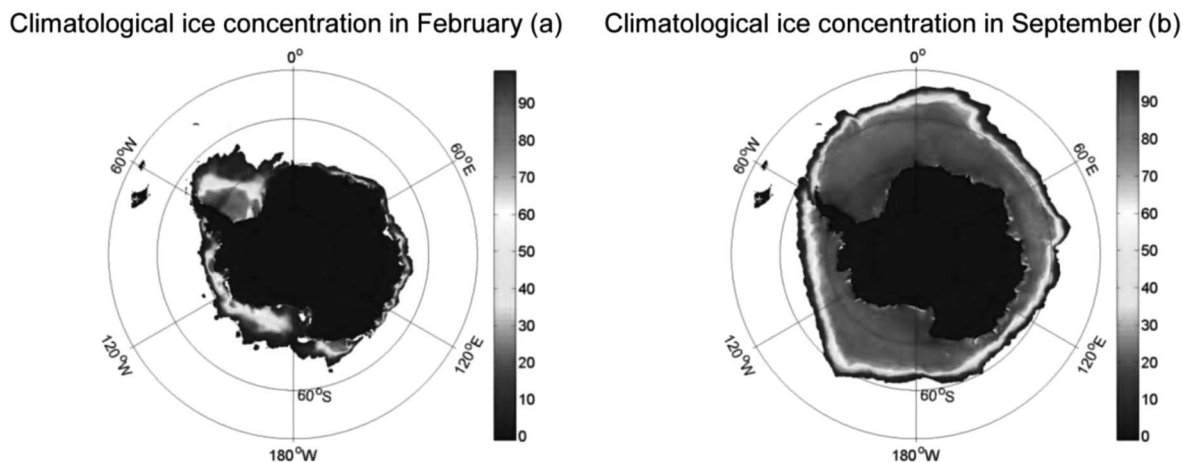


Figure 5. Climatology of Antarctic sea-ice concentration in February (minimum) and September (maximum) from 1991 to 2011. The percentage of sea ice covering the ocean surface is derived from the microwave SSM/I data obtained from the National Snow and Ice Data Center (12.5 km resolution).

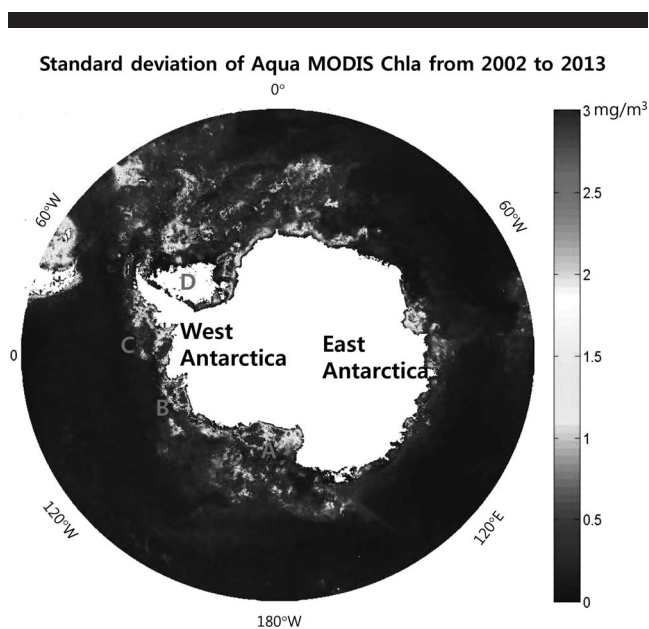


Figure 6. Standard deviation of CHL derived from monthly mean Aqua-MODIS data from July 2002 to March 2013. Areas A through E represent the Ross Sea, the Amundsen Sea, the Bellingshausen Sea, the Ronne Ice Shelf, and the Weddell Sea, respectively.

types (Kuo and Landgrebe, 2002; Mianji and Zhang, 2011): unsupervised classification and supervised classification. For instance, Han *et al.* (2015) reported that hyperspectral imaging is suitable for monitoring the sea ice, which contains continuous spectral information and has superior target-recognition ability. To classify hyperspectral sea-ice images, they used an active-learning (AL) algorithm, which is a neural-network algorithm. The AL algorithm with hyperspectral imaging offers the highest classification accuracy (89.3%) of all algorithms.

Figure 5 illustrates the sea-ice concentration based on SSM/I measurements and shows that the climatological sea-ice concentrations in February (summer) and in September (winter) are very different. The surface area of sea ice exceeded 80% in September, making it about five times higher than that in February. Variations in both sea-ice and ice-shelf coverage around Antarctica play important roles in driving ecological changes. To analyze ecosystem changes due to melting ice, high spatial and spectral resolutions are required. While passive-microwave measurements can identify ice changes over large areas, observations derived from HypsIRI enable ecosystem changes such as CHL and SST to be analyzed in detail.

Figure 6 shows an example of the use of 10 year MODIS CHL standard deviations to examine the biological responses to seasonally melting ice. Higher values of standard deviation appeared in the polynyas, which contain open water from spring to summer but are covered by ice in winter, indicating changes in ocean biology due to seasonal ice melting. Although ice-marginal environments are considered to be among the most important areas for understanding ecosystem changes through climate change, limited observational research has been conducted. The most appropriate remote-sensing tech-

nique for studying the ice-margin environment requires spectral ranges from VSWIR to TIR, which can be enabled by the HypsIRI mission.

Although HypsIRI is an appropriate sensor for studying both thermal and biogeochemical constituents around ice edges, it faces challenges due to its low revisit frequency, low irradiance (and therefore lower SNR for the sensor), and atmospheric-adjacency effects, which may cause stray light to impinge upon the instrument. However, these problems may be compensated by the higher revisit frequency in the polar regions (about 5 days, rather than 16) and the low sun glint at these latitudes.

Shoreline Changes and Floods (Disturbances)

Shoreline changes and floods are also important for estimating marginal disturbances. Thus, extraction of shoreline changes from satellite measurements requires accurate delineation of waterline positions on image time series wherein tidal influences are minimal. Several methods have been proposed and used to derive shoreline positions from passive remote sensing, which may be tested using HypsIRI VSWIR or similar data. These include a single-band method that sets a threshold separating land from water (Bayram *et al.*, 2008), an edge-filter method (Scott *et al.*, 2003), and an unsupervised classification method such as iterative self-organizing data-analysis classification (Armenakis *et al.*, 2003). Similarly, other well-developed indices, including the normalized-difference vegetation index (NDVI), defined as:

$$\text{NDVI} = (R_{\text{NIR}} - R_{\text{RED}}) / (R_{\text{NIR}} + R_{\text{RED}}) \quad (2)$$

where, R is reflectance, and the normalized-difference water index (NDWI), defined as:

$$\text{NDWI} = (R_{\text{GREEN}} - R_{\text{NIR}}) / (R_{\text{GREEN}} + R_{\text{NIR}}) \quad (3)$$

are also used for water/land delineation as well as for flood mapping (Domenikiotis, Loukas, and Dalezios, 2003; Jain *et al.*, 2005; Lunetta *et al.*, 2006; McFeeters, 1996; Ouma and Tateishi, 2006; Xu, 2006). A recently developed index for delineating floating materials in the open ocean, namely, the floating-algae index (Hu, Pichel, and Muller-Karger, 2009), was also found to be effective in delineating the land-water interface (Feng *et al.*, 2012).

While each method in Eq. (2) and (3) has its own pros and cons, the fundamental principle is the same: Water absorbs light strongly in the NIR and SWIR wavelengths, resulting in a much-reduced reflectance compared with other wavelengths for the same image pixels or compared with other pixels for the same wavelengths. For example, the absorption coefficient of water at 1640 nm is 669 m^{-1} . A 1-cm-thick layer of water over a land surface will therefore reduce the land's reflectance to a factor of $\exp(-2 \times 0.01 \times 669) = 0.00015\%$, where the factor of 2 accounts for the two-way light attenuation. Likewise, a 1-mm-thick water lens will reduce the reflectance to about 26%. In other words, single-band images using these wavelengths will appear dark over water and brighter over land. The various methods simply seek efficient ways to extract this information while minimizing the impact of the observing conditions or increasing the computational efficiency.

A recent example of the use of Landsat 30-m-resolution data to document decadal shoreline changes along central Florida's

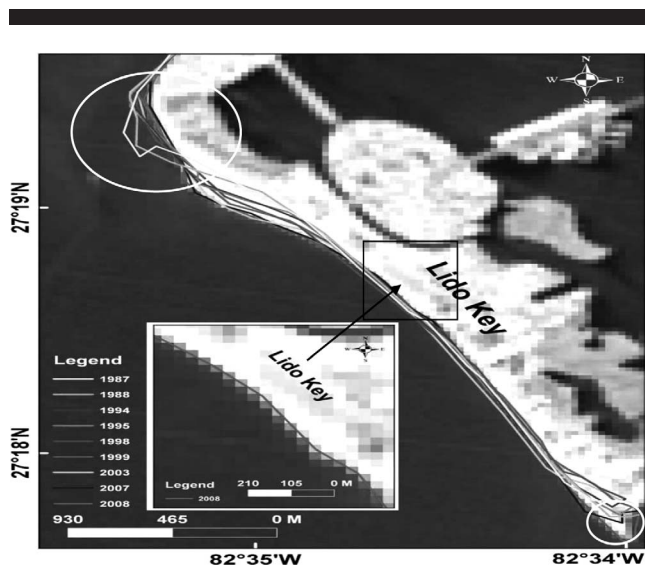


Figure 7. Shoreline delineation from nine Landsat TM images covering central west Florida near Lido Key. The inset image shows an example of how the determined shoreline traces the land-water interface pixels. The two white circles highlight the two shoreline sections that experienced opposite shoreline changes (erosion and accretion). Figure adapted from Yu *et al.* (2011).

west coast is given by Yu *et al.* (2011) (Figure 7). The time-series images were carefully selected to be within a tidal range of ± 9 cm, such that the tidal influence on the shoreline delineation would be known to an accuracy of within 1 Landsat pixel for a shelf slope of 3%–24%. The high-latitude revisit frequency of HyspIRI is close to several days, affording more opportunities than Landsat to observe more rapid changes along the coastlines (Oey *et al.*, 2007).

In addition to Landsat imagery for shoreline detection, Manzoc *et al.* (2015) demonstrated how hyperspectral field radiometry and LIDAR remote sensing can be used to model the effects of varying sediment properties upon reflectance values under both field and laboratory conditions within the field-spectral-libraries, airborne-hyperspectral-images, and topographic-LIDAR (FHyl) procedure using a multisource data set (airborne Hyperspectral– Multispectral Infrared Visible Imaging Spectrometer [MIVIS] and topographic-LIDAR–Hawk-Eye II and field radiometry). The results showed the potential of hyperspectral signals to assess the effects of moisture, grain size, and mineral composition upon sediment properties. This research result suggests that HyspIRI measurements will enable not only shoreline changes to be determined, but also the biogeochemical constituents resulting from disturbances by long-term sea-level changes and short-term hurricane activities.

Furthermore, Smith *et al.* (2004) reported on a study aimed at assessing the suitability of hyperspectral data for estimating mudflat characteristics related to stability, wherein multiple-regression analysis was used to show that hyperspectral images and surface-sedimentary characteristics result in distinct spectral signatures. This result suggests that the use of hyperspectral data for the assessment of erosion, shear

stress, and surface stability (and thus the likely future behavior of this dynamic environment) can contribute to a significant improvement in the information required to successfully manage shallow coastal systems. In addition, Dierssen *et al.* (2003) estimated shallow-water bathymetry and LAI of the seagrass *Thalassia testudinum* using a spectrally based approach. They used two high-resolution images obtained from the Ocean Portable Hyperspectral Imager for Low-Light Spectroscopy (Ocean PHILLS) and found that bathymetry was mapped to meter-scale resolution using a site-specific relationship ($r^2 = 0.97$) derived from spectral ratios of remote-sensing reflectance at 555 and 670 nm. The study also reported that the magnitude of retrieved bottom reflectance was highly correlated to seagrass LAI values within the image as measured from diver surveys ($r^2 = 0.88$ – 0.98).

Thus, the unique capacity of HyspIRI, enabled by its high spectral and spatial resolutions, will significantly enhance current capabilities to accurately map shoreline changes, floods, and shallow bottom bathymetry in targeted areas, providing useful tools for managers, researchers, environmental groups, and the general public to monitor the well-being of coastal zones.

Sensor Characteristics

Until recently hyperspectral sensors have been available only on aircraft (Fearn *et al.*, 2011; Lesser and Mobley, 2007; Li *et al.*, 2006; Ozesmi and Bauer, 2002; Rosso, Ustin, and Hastings, 2005). Imaging spectrometers are now also available in space, as on the Hyperion system. However, Hyperion has a low SNR ratio ($<100:1$; Hu *et al.*, 2012), and the mission is nearing the end of its planned lifetime. HICO had a much higher SNR, yet it was not a global mission, and it recently terminated operation (Table 1).

HyspIRI, on the other hand, is a hyperspectral global mission with a sufficiently high SNR. The projected SNR of HyspIRI (Gao, 2010) is better than that of Hyperion and Landsat (Hu *et al.*, 2012, their Figure 8) or MODIS (Hu *et al.*, 2012, their Figure 7) and comparable to that of HICO (Lucke *et al.*, 2011); this SNR ratio is considered adequate for accurately retrieving hyperspectral reflectance values from the water surface and consequently evaluating aquatic water quality–related properties (Barbier, 2008). Furthermore, compared to HICO measurements, HyspIRI provides additional TIR observations, which are critically important for monitoring thermal variations in coastal regions due to groundwater runoff and river discharges. Therefore, HyspIRI measurements will not only current algorithms for estimating biogeochemical constituents to be improved, but also new algorithms to be developed to study sea-marginal processes.

The 1640 nm band enables highly accurate classification of water and land pixels. However, for shoreline delineation and flood mapping, several practical considerations are necessary to assess HyspIRI's accuracy. The first of these is the geolocation accuracy of the individual pixels on satellite images, which is often on the order of half of a pixel (root mean square [RMS] uncertainties). For example, the highest geolocation accuracy of MODIS data for a nadir view is about 150 m (Wolfe *et al.*, 2002), about half of the 250 m pixel. For Landsat data, the half-pixel accuracy often requires manual

geo-rectification using known ground-control points (e.g., Yu *et al.*, 2011). Assuming that the principle is universal, the HypsIRI land- and water-classification uncertainties will be roughly half a pixel (i.e. about 30 m). The second consideration is the influence of tides, which can range from centimeters to meters, depending on their location. To achieve half-pixel accuracy when delineating shorelines, tidal changes must be restricted to a range that, after accounting for the slope of the intertidal zone, will result in less than a half-pixel uncertainty (Yu *et al.*, 2011). Finally, the third consideration is the revisit frequency. Due to the high spatial-resolution requirements, HypsIRI may revisit the same place less frequently compared with Landsat (16 days at the equator). This not only creates difficulties in finding time-series data that meet the tidal-change constraints for shoreline-change assessment, but it also makes it difficult to perform flooding assessment because the dry/wet conditions over land may change rapidly. Therefore, for noteworthy flood events, the sensor may be tilted to assure rapid response. Overall, although there are some potential limitations to shoreline delineation and flood mapping, it is possible to overcome these difficulties with engineering advancements and algorithm improvements to achieve an RMS accuracy of a half pixel. However, it should be noted that this challenge is lessened at higher latitudes due to more frequent coverage.

In summary, with radiometric capabilities comparable to or better than those of the now-defunct HICO instrument, HypsIRI is more suitable than Landsat for observing the optical characteristics of water (Devred *et al.*, 2013), especially along shallow coastal areas. With its greater spectral range, the HypsIRI mission should provide broader use than could HICO in covering both aquatic and terrestrial features. HypsIRI also offers global coverage, including latitudes above 45 degrees. HypsIRI's eight thermal bands will be more than adequate for observing subtle variations in water-surface temperature, which would be ideal for tracing freshwater or meltwater fluxes along the water-land interface. Its VSWIR spectral capabilities could then observe aquatic-biospheric responses to contemporaneously observed coastal fluxes.

The Hyperion spectrometer on board Earth Observatory 1 (EO-1) is the only true hyperspectral sensor currently in orbit. It has a spectral range and spectral and spatial resolutions comparable to those of HypsIRI, but not extending into the ultraviolet spectrum. However, Hyperion's areal coverage is far from global, and the proof-of-concept mission supported lower radiometric resolutions. Further, the mission is currently scheduled to conclude the EO-1 mission and de-orbit the platform during the 2016 fiscal year, leaving no comparable spaceborne hyperspectral capabilities for Earth observation. The only plans to replace that capability include HypsIRI, the Pre-Aerosol, Clouds and Ecosystems (PACE) mission (<https://pace.oceansciences.org/mission.htm>), and Geostationary Coastal and Air Pollution Events (GeoCAPE) mission (<https://science.jpl.nasa.gov/projects/Geo-Cape/>). With 1000 and 250 m pixels, respectively, PACE and GeoCAPE are far less capable of making observations along the water-land interface. However, their superior temporal resolution could complement HypsIRI observations.

HypsIRI's regular measurements can provide snapshots of global coastal and inland waters. An important strength of HypsIRI for studying these waters is its high spatial and spectral resolutions. Specifically, issues of scale and interactions between complex biophysical dynamics and ecosystem responses could provide input into modeling studies for important biogeochemical constituents.

CONCLUSIONS

The potential applications of the HypsIRI mission to the study of changes in land/water/ice geomorphology have been demonstrated using MODIS, Landsat, and other measurements in this study. Future HypsIRI measurements will provide better information than shown here, due to the mission's improved spatial and spectral resolutions. For the same reasons, although the present discussions have focused upon determining dynamic boundaries, HypsIRI will also improve the accuracy of the retrieved biogeochemical properties of water, leading to better quantification of the environmental changes resulting from short-term and long-term dynamic boundary changes.

ACKNOWLEDGMENTS

This study was supported by NASA through its GeoCAPE and HypsIRI planning efforts. We appreciate useful input from the HypsIRI Aquatic Studies Group, which is sponsored by NASA's Goddard Space Flight Center. This research was a part of the project titled "Ecosystem Structure and Function of Marine Protected Area (MPA) in Antarctica (PM17060)," funded by the Ministry of Oceans and Fisheries, Korea.

LITERATURE CITED

- Ammenberg, P.; Flink, P.; Lindell, T.; Pierson, D., and Strombeck, N., 2002. Bio-optical modelling combined with remote sensing to assess water quality. *International Journal of Remote Sensing*, 23(8), 1621–1638.
- Armenakis, C.; Leduc, F.; Cyr, I.; Savopol, F., and Cavayas, F., 2003. A comparative analysis of scanned maps and imagery for mapping applications. *ISPRS Journal of Photogrammetry and Remote Sensing*, 57(5–6), 304–314.
- Banks, W.S.L.; Paylor, R.L., and Hughes, W.B., 1996. Using thermal infrared imagery to delineate groundwater discharge. *Ground Water*, 43(3), 434–443.
- Barbier, E.B., 2008. Ecosystems as natural assets. *Foundations and Trends in Microeconomics*, 4(8), 611–681.
- Bayram, B.; Acar, U.; Seker, D., and Ari, A., 2008. A novel algorithm for coastline fitting through a case study over the Bosphorus. *Journal of Coastal Research*, 24(4), 983–991.
- Becker, M.W., 2006. Potential for satellite remote sensing of ground water. *Ground Water*, 44(2), 306–318.
- Boehm, A.B.; Shellanbarger, G.G., and Paytan, A., 2004. Groundwater discharge: Potential association with fecal indicator bacteria in the surf zone. *Environment Science and Technology*, 38(13), 3558–3566.
- Boetius, A.; Albrecht, S.; Bakker, K.; Bienhold, C.; Felden, J.; Fernández-Méndez, M.; Hendricks, S.; Katlein, C.; Lalande, C.; Krumpen, T.; Nicolaus, M.; Peeken, I.; Rabe, B.; Rogacheva, A.; Rybakova, E.; Somavilla, R., and Wenzhöfer, F., 2013. Export of algal biomass from the melting arctic sea ice. *Science*, 339(6126), 1430–1432.
- Cendrero, A. and Fischer, D.W., 1997. A procedure for assessing the environmental quality of coastal areas for planning and management. *Journal of Coastal Research*, 13(3), 732–744.

- Chang, S.W.; Clement, T.; Prabhakar, C.; Simpson, M.J., and Lee, K.-K., 2011. Does sea-level rise have an impact on saltwater intrusion. *Advances in Water Resources*, 34(10), 1283–1291.
- Childers, D.L.; Boyer, J.N.; Davis, S.E.; Madden, C.J.; Rudnick, D.T., and Sklar, F.H., 2006. Relating precipitation and water management to nutrient concentrations in the oligotrophic “upside-down” estuaries of the Florida Everglades. *Limnology and Oceanography*, 50(3), 602–616.
- Church, J.A.; Woodworth, P.L.; Aarup, T., and Wilson, W.S. (eds.), 2010. *Understanding Sea-Level Rise and Variability*. Hoboken, New Jersey: Wiley-Blackwell, 428p.
- Chylek, P.; McCabe, M.; Dubey, M.K., and Dozier, J., 2007. Remote sensing of Greenland Ice Sheet using multispectral near-infrared and visible radiances. *Journal of Geophysical Research*, 112(D24), D24S20. doi:10.1029/2007JD008742
- David, R.T., Gao, B.C.; Green, R.O.; Roberts, D.A.; Dennison, P.E., and Lundeen, S.R., 2015. Atmospheric correction for global mapping spectroscopy: ATREM advances for the HyspIRI preparatory campaign. *Remote Sensing of Environment*, 167, 64–77.
- Dekker, A.G.; Malthus, T.J.; Wijnen, M.M., and Seyhan, E., 1992. Remote-sensing as a tool for assessing water-quality in Loosdrecht lakes. *Hydrobiologia*, 233(1–3), 137–159.
- Desantis, L.R.G.; Bhotika, S.; Williams, K., and Putz, F.E., 2007. Sea-level rise and drought interactions accelerate forest decline on the Gulf Coast of Florida, USA. *Global Change Biology*, 13(11), 2349–2360.
- Devred, E.; Turpie, K.R.; Moses, W.; Klemas, V.; Moisan, T.; Babin, M.; Forget, M.-H.; Toro-Farmer, G., and Jo, Y.-H., 2013. Future retrievals of water column bio-optical properties using the Hyperspectral Infrared Imager (HyspIRI). *Remote Sensing*, 5(12), 6812–6837.
- Dierssen, H.M.; Richard, C.; Zimmerman, R.A.; Leathers, T.; Valerie, D., and Curtiss, O.D., 2003. Ocean color remote sensing of seagrass and bathymetry in the Bahamas Banks by high-resolution airborne imagery. *Limnology and Oceanography*, 48(1, part 2), 444–455.
- Domenikiotis, C.; Loukas, A., and Dalezios, N.R., 2003. The use of NOAA/AVHRR satellite data for monitoring and assessment of forest fires and floods. *Natural Hazards and Earth System Science*, 3, 115–128.
- Drüe, C. and Heinemann, G., 2005. Accuracy assessment of sea-ice concentrations from MODIS using *in-situ* measurements. *Remote Sensing of Environment*, 95(2), 139–149.
- Fearn, P.R.C.; Klonowski, W.; Babcock, R.C.; England, P., and Phillips, J., 2011. Shallow water substrate mapping using hyperspectral remote sensing. *Continental Shelf Research*, 31(12), 1249–1259.
- Feng, L.; Hu, C.; Chen, X.; Cai, X.; Tian, L., and Gan, W., 2012. Assessment of inundation changes of Poyang Lake using MODIS observations between 2000 and 2010. *Remote Sensing of Environment*, 121, 80–92.
- Flink, P.; Lindell, T., and Ostlund, C., 2001. Statistical analysis of hyperspectral data from two Swedish lakes. *Science of the Total Environment*, 268(1–3), 155–169.
- Galvao, L.S.; Pereira Filho, W.; Abdon, M.M.; Novo, E.M.M.L.; Silva, J.S.V., and Ponzoni, F.J., 2003. Spectral reflectance characterization of shallow lakes from the Brazilian Pantanal wetlands with field and airborne hyperspectral data. *International Journal of Remote Sensing*, 24(21), 4093–4112.
- Gao, B.-C., 2010. *HyspIRI Visible to Short Wavelength Infrared (VSWIR) Water Leaving Reflectance Algorithm Theoretical Basis Document (ATBD)*. <http://hyspirci.jpl.nasa.gov/>
- Garcia, C.A.; Purdie, D.A., and Robinson, I.S., 1993. Mapping a bloom of the photosynthetic ciliate *Mesodinium rubrum* in an estuary from airborne thematic mapper data. *Estuarine, Coastal and Shelf Science*, 37(3), 287–298.
- Gould, R.W. and Arnone, R.A., 1997. Remote sensing estimates of inherent optical properties in a coastal environment. *Remote Sensing of Environment*, 61(2), 290–301.
- Grose, R.D.; Michaelsen, J.C.; Doohar, B.P.; MacQueen, D.H.; Cullen, S.J.; Kastenber, W.E., and Marino, M.A., 1995. *California Leaking Underground Fuel Tank (LUFT) Historical Case Analyses* (p. 20). Livermore, California: Lawrence Livermore National Laboratory, Environmental Protection Department, Environmental Restoration Division, <https://www.waterboards.ca.gov/ust/cleanup/docs/lnlplum.pdf>, 65p.
- Hakvoort, H.; deHaan, J.; Jordans, R.; Vos, R.; Peters, S., and Rijkeboer M., 2002. Towards airborne remote sensing of water quality in the Netherlands—Validation and error analysis. *Journal of Photogrammetry and Remote Sensing*, 57(3), 171–183.
- Han, Yanling; Ren, J.; Hong, Z.; Zhang, Y.; Zhang, L.; Meng, W., and Gu, Q., 2015. Active learning algorithms for the classification of hyperspectral sea ice images. *Mathematical Problems in Engineering*, 2015, Article ID 124601, 10p.
- Hildebrandt, A.; Guillaumon, M.; Lacorte, S.; Tauler, R., and Barceló, D., 2008. Impact of pesticides used in agriculture and vineyards to surface and groundwater quality (north Spain). *Water Research*, 42(13), 3315–3326.
- Hochberg, E.J.; Roberts, D.A.; Dennison, P.E., and Hulley, G.C., 2015. Special Issue on the Hyperspectral Infrared Imager (HyspIRI). *Remote Sensing of Environment*, 167, 1–280.
- Hoja, D.; Lehner, S.; Niedermeier, A., and Romaneessen, E., 2000. DEM generation from ERS SAR shorelines compared to airborne crosstrack InSAR DEMs in the German Bight. *Proceedings of the 20th International Geoscience and Remote Sensing Symposium* (Honolulu, Hawaii, July 24–28), Volume 5, pp. 1889–1891.
- Hu, C.; Feng, L.; Lee, Z.; Davis, C.O.; Mannino, A.; McClain, C.R., and Franz, B.A., 2012. Dynamic range and sensitivity requirements of satellite ocean color sensors: Learning from the past. *Applied Optics*, 51(25), 6045–6062.
- Hu, C.; Li, X.; Pichel, W.G., and Muller-Karger, F.E., 2009. Detection of natural oil slicks in the NW Gulf of Mexico using MODIS imagery. *Geophysical Research Letters*, 36(1), L01604.
- Hu, C.; Muller-Karger, F.E., and Swarzenski, P.W., 2006. Hurricanes, submarine groundwater discharge and Florida’s red tides. *Geophysical Research Letters*, 33(11), L11601.
- HyspIRI-TIR Science Working Group Report, 2007. *Thermal Infrared Multispectral Scanner NASA Mission Concept Study*. <http://calval.jpl.nasa.gov/hyspirci>
- Jain, S.K.; Singh, R.D.; Jain, M.K., and Lohani, A K., 2005. Delineation of flood-prone areas using remote sensing techniques. *Water Resources Management*, 19(4), 333–347.
- Johnson, A.G.; Glenn, C.R.; Burnett, W.C.; Peterson, R., and Lucey, P.G., 2008. Aerial infrared imaging reveals large nutrient-rich groundwater inputs to the ocean. *Geophysical Research Letters*, 35(15), 1–6.
- Kallio, K.; Kutseer, T.; Hanonen, T.; Koponen, S.; Pulliainen, J.; Vepsäläinen, J., and Pyhälähti, T., 2001. Retrieval of water quality from airborne imaging spectrometry of various lake types in different seasons. *Science of the Total Environment*, 268(1–3), 59–77.
- Kanai, Y.; Ueta, M.; Germogenov, N.; Nagendran, M.; Mita, N., and Higuichi, H., 2002. Migration routes and important resting areas of Siberian cranes (*Grus leucogeranus*) between northeastern Siberia and China as revealed by satellite tracking. *Biological Conservation*, 106(3), 339–346.
- Klemas V., 2009. The role of remote sensing in predicting and determining coastal storm impacts. *Journal of Coastal Research*, 25(6), 1264–1275.
- Kolokoussis, P.; Karathanassi, V.; Rokos, D.; Argialas, D.; Karageorgis, A.P., and Georgopoulos, D., 2011. Integrating thermal and hyperspectral remote sensing for the detection of coastal springs and submarine groundwater discharges. *International Journal of Remote Sensing*, 32(23), 8231–8251.
- Konstantinou, I.K.; Hela, D.G., and Albanis, T.A., 2006. The status of pesticide pollution in surface waters (rivers and lakes) of Greece. Part I. Review on occurrence and levels. *Environmental Pollution*, 141(3), 555–570.
- Kuo, B.C. and Landgrebe, D.A., 2002. A robust classification procedure based on mixture classifiers and nonparametric weighted feature extraction. *IEEE Transactions on Geoscience and Remote Sensing*, 40(11), 2486–2494.
- LaValle, P.D. and Lakhani, V.C., 2000. An assessment of lake level fluctuations on beach and shoreline changes. *Coastal Management*, 28(2), 161–173.

- Lee, I.-C.; Cheng, L., and Li, R., 2010. Optimal parameter determination for mean-shift segmentation-based shoreline extraction using LiDAR data, aerial orthophotos, and satellite imagery. *Proceedings of the American Society for Photogrammetry and Remote Sensing (ASPRS) 2010 Annual Conference* (San Diego, California, 26–30 April), 8p.
- Lee, I.-C.; Wu, B., and Li, R., 2009. Shoreline extraction from the integration of LiDAR point cloud data and aerial orthophotos using mean shift segmentation. *Proceedings of the American Society for Photogrammetry and Remote Sensing (ASPRS) 2009 Annual Conference* (Baltimore, Maryland), p. 489.
- Lee, S.H.; Stockwell, D.A.; Joo, H.-M.; Son, Y.B.; Kang, C.-K., and Whittlege, T.E., 2012. Phytoplankton production from melting ponds on Arctic sea ice. *Journal of Geophysical Research*, 117(C4), C04030.
- Lee, Y.-W. and Kim, G., 2007. Linking groundwater-borne nutrients and dinoflagellate red-tide outbreaks in the southern sea of Korea using a Ra tracer. *Estuarine, Coastal and Shelf Science*, 71(1), 309–317.
- Lee, Z.; Carder, K.L.; Hawes, S.K.; Steward, R.G.; Peacock, T.G., and Davis, C.O., 1994. Model for the interpretation of hyperspectral remote-sensing reflectance. *Applied Optics*, 33(24), 5721–5732.
- Leote, C.; Ibanhez Severino, J., and Rocha, C., 2008. Submarine groundwater discharge as a nitrogen source to the Ria Formosa studied with seepage metres. *Biogeochemistry*, 88(2), 185–194.
- Lesser, M.P. and Mobley, C.D., 2007. Bathymetry, water optical properties, and benthic classification of coral reefs using hyperspectral remote sensing imagery. *Coral Reefs*, 26(4), 819–829.
- Li, R.; Bedford, K.W.; Niu, X.; Velissariou, V.; Zhou, F., and Deshpande, S., 2006. *Seamless Integration of Geospatial Data from Water to Land, Annual Project Report (2nd Year)*. National Geospatial-Intelligence Agency, December 2006, 43p.
- Li, R.; Ma, R., and Di, K., 2002. Digital tide-coordinated shorelines. *Journal of Marine Geodesy*, 25(1–2), 27–36.
- Liu, H.; Sherman, D., and Gu, S., 2007. Automated extraction of shorelines from airborne light detection and ranging data and accuracy assessment based on Monte Carlo simulation. *Journal of Coastal Research*, 23(6), 1359–1369.
- Lucke, R.L.; Corson, M.; McGlothlin, N.R.; Butcher, S.D.; Wood, D.L.; Korwan, D.R.; Li, R.R.; Snyder, W.A.; Davis, C.O., and Chen, D.T., 2011. Hyperspectral Imager for the Coastal Ocean: Instrument description and first images. *Applied Optics*, 50(11), 1501–1516.
- Lunetta, R.S.; Knight, J.F.; Ediriwickrema, J.; Lyon, J.G., and Worthy, L.D., 2006. Land-cover change detection using multi-temporal MODIS NDVI data. *Remote Sensing of Environment*, 105(2), 142–154.
- Manzoc, C.; Valentinia, E.; Taramellia, A.; Filipponia, F., and Disperatib, L., 2015. Spectral characterization of coastal sediments using Field Spectral Libraries, Airborne Hyperspectral Images and Topographic LiDAR Data (FHyL). *International Journal of Applied Earth Observation and Geoinformation*, 36, 54–68.
- Mason, D.C.; Davenport, I.J., and Flather, R.A., 1997. Interpolation of an intertidal digital elevation model from heighted shorelines: A case study in the western Wash. *Estuarine, Coastal, and Shelf Science*, 45(5), 599–612.
- Mason, D.C.; Davenport, I.J.; Flather, R.A., and Gurney, C., 1998. A digital elevation model of the intertidal areas of the Wash produced by the waterline method. *International Journal of Remote Sensing*, 19(8), 1455–1460.
- Mason, D.C.; Davenport, I.J.; Flather, R.A.; Gurney, C.; Robinson, G.J., and Smith, J.A., 2001. A sensitivity analysis of the waterline method of constructing a digital elevation model for intertidal areas in ERS SAR scene of eastern England. *Estuarine, Coastal, and Shelf Science*, 53(6), 759–778.
- Mason, D.C.; Davenport, I.J.; Robinson, G.J.; Flather, R.A., and McCartney, B.S., 1995. Construction of an inter-tidal digital elevation model by the 'water-line' method. *Geophysical Research Letters*, 22(23), 3187–3190.
- McFeeters, S.K., 1996. The use of the Normalized Difference Water Index (NDWI) in the delineation of open water features. *International Journal of Remote Sensing*, 17(7), 1425–1432.
- McKenna, T.; Andres, A.; Wang, L.T., and DeLiberty, T., 2001. Mapping locations of ground-water discharge in Rehoboth and Indian River bays, Delaware, using thermal imagery. *Geological Society of America Abstracts with Programs*, 33, 44.
- Meyer, F.J.; Mahoney, A.R.; Eicken, H.; Denny, C.L.; Druckenmiller, H.C., and Hendricks, S., 2011. Mapping Arctic land fast ice extent using L-band synthetic aperture radar interferometry. *Remote Sensing of Environment*, 115(12), 3029–3043.
- Mianji, F.A. and Zhang, Y., 2011. Robust hyperspectral classification using relevance vector machine. *IEEE Transactions on Geoscience and Remote Sensing*, 49(6), 2100–2112.
- Morton, R.A.; Leach, M.P.; Paine, J.G., and Cardoza, M.A., 1993. Monitoring beach changes using GPS surveying techniques. *Journal of Coastal Research*, 9(3), 702–720.
- Moseley, C.L. and Meyer, M.R., 1992. Petroleum contamination of an elementary school: A case history involving air, soil-gas, and groundwater monitoring. *Environmental Science and Technology*, 26(1), 185–192.
- Muller-Karger, F.E., 1984. Lower Trophic Level Studies in the Marginal Sea Ice Zone. Fairbanks, Alaska: University of Alaska, Master's thesis, 145p.
- Muller-Karger, F.E. and Alexander, V., 1987. Nitrogen dynamics in a marginal sea-ice zone. *Continental Shelf Research*, 7(7), 805–823.
- Muller-Karger, F.E.; McClain, C.R., and Ray, C.C., 1987. Primary productivity. In: *Strategic Atlas of Economic Resources of the Bering Sea*. Rockville, Maryland: NOAA Strategic Assessment Branch.
- Muller-Karger, F.E.; McClain, C.R.; Sambrotto, R.N., and Ray, C.G., 1990. Measurements of phytoplankton distribution in the south-eastern Bering Sea using the CZCS: A note of caution. *Journal of Geophysical Research*, 95(C7), 11483–11499.
- Muslim, A.M. and Foody, G.M., 2008. DEM and bathymetry estimation for mapping a tide-coordinated shoreline from fine spatial resolution satellite sensor imagery. *International Journal of Remote Sensing*, 29(15), 4515–4536.
- Nowack, B.; Xue, H., and Sigg, L., 1997. Influence of natural and anthropogenic ligands on metal transport during infiltration of river water to groundwater. *Environmental Science and Technology*, 31(3), 866–872.
- Oey, L.-Y.; Ezer, T.; Hu, C., and Muller-Karger, F.E., 2007. Baroclinic tidal flows and inundation processes in Cook Inlet, Alaska: Numerical modeling and satellite observations. *Ocean Dynamics*, 57(3), 205–221.
- Ostlund, C.; Flink, P.; Strombeck, N.; Pierson, D., and Lindell, T., 2001. Mapping of the water quality of Lake Erken, Sweden, from imaging spectrometry and Landsat Thematic Mapper. *Science of the Total Environment*, 268(1–3), 139–154.
- Ouma, Y.O. and Tateishi, R., 2006. A water index for rapid mapping of shoreline changes of five East African Rift Valley lakes: An empirical analysis using Landsat TM and ETM+ data. *International Journal of Remote Sensing*, 27(15), 3153–3181.
- Ozesmi, S.L. and Bauer, M.E., 2002. Satellite remote sensing of wetlands. *Wetlands Ecology and Management*, 10(5), 381–402.
- Ozsoy-Cicek, B.; Ackley, S.F.; Worby, A.; Xie, H., and Lieser, J., 2011. Antarctic sea-ice extents and concentrations: Comparison of satellite and ship measurements from International Polar Year cruises. *Annals of Glaciology*, 52(57), 318–326.
- Perrette, M.; Yool, A.; Quartly, G.D., and Popova, E.E., 2011. Near-ubiquity of ice-edge blooms in the Arctic. *Biogeosciences*, 8, 515–524.
- Portnoy, J.W.; Nowicki, B.L.; Roman, C.T., and Urish, D.W., 1998. The discharge of nitrate-contaminated groundwater from developed shoreline to marsh-fringed estuary. *Water Resources Research*, 34(11), 3095–3104.
- Robertson, W.V.; Whitman, D.; Zhang, K.Q., and Leatherman, S.P., 2004. Mapping shoreline position using airborne laser altimetry. *Journal of Coastal Research*, 20(3), 884–892.
- Roseen, R.M.; Brannaka, L.K., and Ballestero, T.P., 2001. Determination of nutrient loading from groundwater discharge into an inland estuary using airborne thermal imagery. *Proceedings of the 12th Biennial Coastal Zone Conference* (Cleveland, Ohio), pp. 1–4.

- Rosso, P.H.; Ustin, S.L., and Hastings, A., 2005. Mapping marshland vegetation of San Francisco Bay, California, using hyperspectral data. *International Journal of Remote Sensing*, 26(23), 5169–5191.
- Sangodoyin, A.Y. and Agbawhe, O.M., 1992. Environmental study on surface and groundwater pollutants from abattoir effluents. *Bioresource Technology*, 41(3), 193–200.
- Schubert, M.; Scholten, J.; Schmidt, A.; François Comanducci, J.; Pham, M.K.; Mallast, U., and Knoeller, K., 2014. Submarine groundwater discharge at a single spot location: Evaluation of different detection approaches. *Water*, 6(3), 584–601.
- Scott, J.W.; Moore, L.R.; Harris, W.M., and Reed, M.D., 2003. *Using the Landsat 7 Enhanced Thematic Mapper Tasseled Cap Transformation to Extract Shoreline*. Rolla, Missouri: U.S. Geological Survey, *Open-File Report 03-272*, 14p.
- Shi, J.; Guo, J.; Zheng, T.; Wang, Q., and Zhu, J., 2012. Monitoring sea ice based on NOAA/AVHRR data in Earth Observing Systems XVII. *Proceedings of SPIE*, 8510, 85100Z.
- Smith, G.M.; Thomson, A.G.; Moöller, I., and Kromkamp, J.C., 2004. Using hyperspectral imaging for the assessment of mudflat surface stability. *Journal of Coastal Research*, 20(4), 1165–1175.
- Song, Y.T. and Colberg, F., 2011. Deep ocean warming assessed from altimeters, Gravity Recovery and Climate Experiment, *in situ* measurements, and a non-Boussinesq ocean general circulation model. *Journal of Geophysical Research*, 116(C2), C02020.
- Stammer, D.; Cazenave, A.; Ponte, R.M., and Tamisiea, M.E., 2013. Causes for contemporary regional sea level changes. *Annual Review of Marine Science*, 5, 21–46.
- Stauble, D.K., 2003. The use of shoreline change mapping in coastal engineering project assessment. In: Byrnes, M.R.; Crowell, M., and Fowler, C. (eds.), *Shoreline Mapping and Change Analysis: Technical Considerations and Management Implications*. *Journal of Coastal Research*, Special Issue No. 38, pp. 178–206.
- Stockdon, H.F.; Sallenger, A.H.; List, J.H., and Holman, R.A., 2002. Estimation of shoreline position and change using airborne topographic LIDAR data. *Journal of Coastal Research*, 18(3), 502–513.
- Ullman, W.J. and Miller, D.C., 2004. Ecological consequences of ground water discharge to Delaware Bay, United States. *Ground Water*, 42(7), 959–970.
- Wang, L.T.; McKenna, T.E., and DeLiberty, T.L., 2008. *Locating Ground-Water Discharge Areas in Rehoboth and Indian River Bays and Indian River Delaware using Landsat 7 Imagery*. Newark, Delaware: Delaware Geological Survey, *Report of Investigations 74*, 17p.
- White, S., 2007. Utilization of LiDAR and NOAA's Vertical Datum Transformation Tool (VDatum) for shoreline delineation. *Proceedings of the Marine Technology Society/IEEE OCEANS Conference* (Vancouver, British Columbia, Canada), 6p.
- White, S.A.; Parrish, C.E.; Calder, B.R.; Pe'eri, S., and Rzhano, Y., 2010. LIDAR-derived national shoreline: Empirical and stochastic uncertainty analysis. In: Pe'eri, S. and Long, B. (eds.), *Applied LIDAR Techniques*. *Journal of Coastal Research*, Special Issue No. 62, pp. 62–74.
- Wolfe, R.E.; Nishihama, M.; Fleig, A.J.; Kuyper, J.A.; Roy, D.P.; Storey, J.C., and Patt, F.S., 2002. Achieving sub-pixel geolocation accuracy in support of MODIS land science. *Remote Sensing of Environment*, 83(1–2), 31–49.
- Wu, W., 2007. Coastline evolution monitoring and estimation—A case study in the region of Nouakchott, Mauritania. *International Journal of Remote Sensing*, 28(24), 5461–5484.
- Xu, H., 2006. Modification of Normalized Difference Water Index (NDWI) to enhance open water features in remotely sensed imagery. *International Journal of Remote Sensing*, 27(14), 3025–3033.
- Yang, D. and Pan, D., 2007. Hyperspectral retrieval model of phyocyanin in case II waters. *Chinese Science Bulletin*, 51(S2), 149–153.
- Jeremy, M.; Beaudoin, A.; Beaudoin, J.D., and Walter, G.M., 2001. *Global Shoreline Mapping from an Airborne Polarimetric SAR: Assessment for RADARSAT 2 Polarimetric Mode*. Ottawa, Canada: Defence Research Establishment, 67p.
- Yu, K.; Hu, C.; Muller-Karger, F.E.; Lu, D., and Soto, I., 2011. Shoreline changes in west-central Florida between 1987 and 2008 from Landsat observations. *International Journal of Remote Sensing*, 32(23), 8299–8313.
- Zimmerman, G. and Bijker, W., 2004. Monitoring the Amazon with different spatial and temporal resolution. *XX ISPRS Congress Proceedings* (Istanbul, Turkey, July 2004), 5p.